

Modeling The Multiwavelength Spectra of Blazars

S. Gasparyan[†]

[†] ICRA Net Armenia Marshall Baghramian Avenue 24a, 0019 Yerevan, Republic of Armenia
E-mail: sargisgyan@gmail.com

Received 28 February 2019

Abstract. The observations of astrophysical sources in a large frequency range (from radio to very high energy gamma-ray bands) provide complete information on the nonthermal processes taking place in different objects. The modeling of acquired data is crucial for understanding the particle acceleration and emission processes. In this paper a new code that can derive the model free parameters that statistically best describe the observed data is presented. It derives the best-fit parameters and their uncertainties through Markov Chain Monte Carlo sampling of the likelihood distributions. Various processes for the cooling of electrons are included in the code which allows its wide application. The code is applied to model the broadband spectral energy distributions of two well-known blazars – Mkn 501 and PKS 0537-441. Using the obtained parameters, the physical processes in their relativistic jets are discussed.

Keywords: Blazars, gamma-rays, relativistic particles in jets, nonthermal emission, theoretical modeling

1. Introduction

Since there are a large number of telescopes currently operating in different bands, the physical processes taking place in astrophysical sources can be investigated by measuring their emission spectra in a large frequency range. These multiwavelength observations are crucial as they allow not only to investigate the emission features in a single band, but also provide a global picture of radiation processes from low (radio band) to high energy (HE ; $> 100 MeV$) bands.

Currently there are various source classes (both Galactic and extragalactic) that are confirmed to have nonthermal spectra extending up to HE or very HE γ -ray bands. Among these sources active galactic nuclei are constantly emitting for a very long period ($> 10^7$ yr) which makes them one of the most powerful long-lived objects in the Universe [1]. Up to date different types of AGNs are confirmed to be strong nonthermal emitters among which most interesting ones are blazars - an extreme class of AGNs, when the jet makes a small viewing angle in respect to the line of sight [2]. Due to small inclination angle and large bulk motion, the emission from blazars is affected by relativistic beaming, which significantly increases the observed luminosity. Blazars conventionally are divided into two sub-classes, BL Lacertae objects (BL-Lacs) and Flat Spectrum Radio Quasars (FSRQs), based on observational features. BL-Lacs have very weak or no emission lines unlike the FSRQs, which have stronger emission lines and a very powerful accretion disk (so powerful, that its thermal emission sometimes can be observed) [2]. Blazars have been subjects of investigation since their discovery, but several crucial problems for understanding their physics are still unclear. For example, how the jets are formed and remain collimated over large distances?, what are the particle acceleration and emission processes?, where does the emission originate along the jet? etc.

There are different ways to investigate the physics of blazar jets. It is believed, that theoretical modeling of the observed multiwavelength spectral energy distributions (SEDs) is a powerful

tool to infer different unknown parameters of the jet. For example, the theoretical modeling will allow to estimate or, at least, constrain the emitting particle energy density and distribution, magnetic field, jet luminosity, etc., which are necessary to investigate the physics of the jets. As all the proposed models contain several free parameters with the increase of the available multiwavelength data and its quality, now one of the most actual problems is to find the parameters that statistically best describe the data. There are a number of different methods and tools available, which can, in some order, help to solve the problem of optimization of parameters during the fitting: for example, the online software developed by Tramacere et al. [3][4], which does not apply statistical approach to constrain the model and it should be done manually. Other advanced methods include calculation of various statistical functions such as chi-square (χ^2), log-likelihood ($\ln \mathcal{L}$) and/or Bayesian Information Criterion (BIC), which are applied to different models allowing to select the one that best explains the data. Here, a new code that can be used to fit the multiwavelength SEDs of blazars, which uses Markov Chain Monte Carlo (MCMC) method, is described.

The code uses *Naima* package [5] which compares the model for nonthermal radiation of relativistic particles with the data and finds the best guess values for the model free parameters. This can be an efficient method for the models with a large number of free parameters.

This paper is structured as follows: the mechanisms for broadband emission from blazar jets are described in Sect. 2; the structure of the code as well as the radiative models and nonthermal spectra of electrons are described in Sect. 3; the code is applied to model the SEDs of two well-known blazars – Mkn 501 (BL-Lac) and PKS 0537-441 in Sec. 4; and the Results and Discussion are presented in Sect. 5.

2. Broadband emission from blazars

The electromagnetic emission from blazars is observed in a wide energy range from radio to HE γ -ray bands. This broadband emission is predominantly of a nonthermal origin, although, sometimes, thermal emission from some components can be also observed. The broadband SED of blazars has two nonthermal peaks - one at optical/UV or X-rays (the low-energy component) and the other at higher energies (the γ -ray band). The observed high-degree polarization indicates that the low-energy component is most likely due to the synchrotron emission of electrons accelerated in the jet. Depending on the peak of the synchrotron emission, blazars can be further divided into low- (LBL: $\nu_s < 10^{14} \text{ Hz}$), intermediate- (IBL: $10^{14} \text{ Hz} < \nu_s < 10^{15} \text{ Hz}$) and high-energy peaked sources ($\nu_s > 10^{15} \text{ Hz}$) [6]. While the synchrotron emission can explain the observed features of the low-energy component, the origin of the HE component is still unclear, so various models/scenarios were proposed. One of the most widely applied models is that the HE component is produced via inverse-Compton (IC) scattering of soft photons being either internal (e.g., synchrotron photons [SSC]) [7][8] or external (EIC) [9][10] to the jet. These models have been successful in explaining the SEDs of blazars but sometimes fail to reproduce some observed features. As a distinct alternative, models involving the radiative output of protons accelerated in the jet (hadronic models) were proposed [11][12]. The protons carry significant amount of energy and the exact estimation of their content in the jet can be crucial for

understanding the physics of the jet. Even in the leptonic scenarios, hadrons (protons) are expected to be present in the jet to ensure the charge neutrality of the plasma. Then these protons can be effectively accelerated and by interacting with a dense target (proton-proton interaction), magnetic (proton-synchrotron) and/or photon fields ($p\gamma$ interaction) produce the observed HE component. In the case of hadronic models, more extreme parameters are required as compared with leptonic models (e.g., in the last two cases the protons should be accelerated beyond 10^{19} eV and propagate in a magnetic field exceeding $30G$ [12][13][14]) but in principle these conditions can be formed in the jet and sometimes the hadronic models give better modeling of SEDs [15][16].

Leptonic one-zone emission scenarios are the most common models applied to explain the broadband emission from blazars. The emitting region is assumed to have a spherical geometry (blob) carrying a magnetic field with an intensity of B and a population of relativistic electrons/positrons. Since the emission region moves along the jet with a bulk Lorentz factor of Γ_{bulk} , the observed radiation will be amplified by a relativistic Doppler factor of $\delta = 1/\Gamma_{bulk}(1 - \beta \cos(\Theta_{obs}))$, where Θ_{obs} is the jet inclination angle (usually $< 8^\circ$ for blazars). The size of emission region can be constrained by the observed variability time-scale (τ), $R_b \leq \delta c\tau/(1+z)$. It has already been noted that blazars are characterized by extreme variability (in both time and amplitude), which implies that the emission region should be very compact. For typical parameters of $t_{var} \sim$ few hours and $\delta \sim 10 \div 20$, the emission region cannot exceed $10^{15} - 10^{16}$ cm. This implies that blazar observations are unique tools for investigation of the sub-parsec structures of their jets.

When the emitting region propagates along the jet, the electrons emit via synchrotron emission and IC up scatter soft photons, producing the observed multiwavelength spectra. Depending on the distance from the central source, different photon fields can serve as targets for IC scattering [17]. Due to compactness of the emitting region, the synchrotron photons themselves can be up scattered to higher energies (SSC). However, sometimes the energy density of photons reflected from the broad-line region or emitted from the infrared dusty torus can exceed the synchrotron ones, so the HE emission can be explained as IC scattering of those external photons (EIC). As the one-zone models assume the emission is produced from a single population of electrons, it is expected to have correlated flux changes in various bands [18]. However, for some blazars the expected correlations were not observed, so alternative two-zone models were proposed [19]. The basic idea of two-zone models is that the multiwavelength emission is produced from two blobs having different size or location along the jet and each containing different population of particles. For example, one of these models assumes that particles are accelerated in one blob, but they emit whenever they are injected in the second blob. As an alternative, in order to explain the rapid variability in the γ -ray band, a model where the emission is produced in two emitting regions of different sizes and distances from the central source was proposed. Of course, two-zone models contain more free parameters, so are easier for modeling, but these are only possibilities, when complex changes of multiwavelength flux are observed.

3. Fitting the multiwavelength SEDs of blazars

Every applied theory contains several free parameters that cannot be constrained by the observations. One of the most actual problems in the fitting of the multiwavelength SEDs is to find parameters that statistically best describe the observed data. There are different methods applied to optimize the parameter space, the simplest one being χ^2 minimization. However, this is not efficient for the model containing many free parameters, so much more complex methods should be applied. Below the code that performs optimization of free parameters, using MCMC method, is described.

3.1 Code description

In order to optimize the free parameters when modeling SEDs, a python code was developed. It is based on the *Naima* package [5] which enables to constrain a model's free parameters by performing MCMC fitting. The MCMC approach, which is based on the Bayesian statistics, is superior to the grid approach with a more efficient sampling of the parameter space of interest, especially for high dimensions [20]. The algorithm behind the code is the affine-invariant ensemble sampling algorithm for MCMC method proposed by Goodman & Weare [21], which has several advantages over traditional MCMC sampling methods (e.g. the Metropolis-Hastings algorithm) and excellent performance as measured by the autocorrelation time [22]. The code derives the best-fit model and uncertainty distributions of spectral model parameters through MCMC sampling of their likelihood distributions. The measurements and uncertainties in the observed data are assumed to be correct, Gaussian, and independent [5]. Under this assumption, the likelihood of the observed data given the spectral model $S(\vec{p}; E)$, for a parameter vector \vec{p} , is

$$\mathcal{L} = \prod_{i=1}^N \frac{1}{\sqrt{2\pi\sigma_i^2}} \exp\left(-\frac{(S(\vec{p}; E_i) - F_i)^2}{2\sigma_i^2}\right), \quad (1)$$

where (F_i, σ_i) are the flux measurement and uncertainty at E_i over N spectral measurements. The corresponding log-likelihood will be:

$$\ln \mathcal{L} = K - \sum_{i=1}^N \frac{(S(\vec{p}; E_i) - F_i)^2}{2\sigma_i^2} \quad (2)$$

Given that the MCMC procedure will sample the areas of the distribution with maximum value of the objective function, it is useful to define the objective function as the log-likelihood disregarding the constant factor:

$$\ln \mathcal{L} \propto \sum_{i=1}^N \frac{(S(\vec{p}; E_i) - F_i)^2}{2\sigma_i^2} \quad (3)$$

The $\ln \mathcal{L}$ function in this assumption can be related to the χ^2 parameter as $\chi^2 = -2 \ln \mathcal{L}$, so that maximization of the log-likelihood is equivalent to the minimization of χ^2 [5]. More about MCMC or the sampling algorithm can be found in [23] and [22]. In addition to the likelihood from the data points, a prior likelihood for all free parameters should be considered. This prior likelihood should be constrained using our knowledge of parameters, for example if it can be inferred from observed parameters or from previous modeling. The combination of the prior and data likelihood functions are used to initiate MCMC run to find parameters best describing the data.

3.2 Radiative models

The prepared package consists of three major sub-packages: *radiative models*- where all cross-sections of electron interaction are defined, *electron spectral models*- where all possible electron spectra expected from their acceleration and cooling are defined, and *optimization* sub-package- that optimize the model free parameters. Each of them should be properly defined before running the program.

Radiative models: The electrons in the jet of blazars primarily lose energy via synchrotron emission. In a magnetic field B , the synchrotron luminosity of electron population with $N(E_e)$ energy distribution is calculated as [24]

$$L_{syn}(E_\gamma) = \frac{\sqrt{3}}{2\pi} \frac{e^3 B}{m_e c^2 \hbar} E_\gamma \int_{E_{e,min}}^{E_{e,max}} N(E_e) G\left(\frac{E_\gamma}{E_c}\right) dE_e, \quad (4)$$

where E_e, m_e, e are the electron energy, rest mass, and charge, respectively;

$E_c = \frac{3eB}{4\pi m_e c} \left(\frac{E_e}{m_e c^2}\right)^2$ is the characteristic energy of emitted synchrotron photons, and $G(x)$ is given by (an approximation of integrals with the Bessel's functions)

$$G(x) \approx \frac{1.808x^{1/3}}{\sqrt{1+3.4x^{2/3}}} \frac{1+2.21x^{2/3}+0.347x^{4/3}}{1+1.353x^{2/3}+0.217x^{4/3}} e^{-x}. \quad (5)$$

The second mechanism used in the modeling of blazar SEDs is IC up scattering of low-energy photons. The luminosity of IC radiation of electron population in a photon field with a density of $u(\varepsilon)$ can be computed by

$$L_{IC}(E_\gamma) = \frac{3}{4} \frac{c\sigma_T}{m_e c^2} E_\gamma^2 \int_0^\infty d\varepsilon \frac{u(\varepsilon)}{\varepsilon^2} \int_{E_{e,min}}^{E_{e,max}} dE_e \frac{N(E_e)}{E_e^2} F_C(E_\gamma, \varepsilon, \gamma), \quad (6)$$

where σ_T - is the Thomson cross-section, ε and E_γ are the photon energies before and after the scattering and $F_C(E_\gamma, \varepsilon, \gamma)$ is the monochromatic differential cross section [25]. In the case of SSC radiation, $u(\varepsilon)$ corresponds to the density of synchrotron photons and it can be straightforwardly computed from equation (4) with

$$u_{SSC} = \frac{2.24 L_{syn}}{4\pi c R_{blob}^2}. \quad (7)$$

In the case of EIC emission, the photons reflected from BLR or infrared emission from the dusty torus can be selected as target photon fields (direct radiation of the accretion disk surrounding the central source has small contribution). The density of these external photons can be calculated by [17][26] :

$$u(r) = \frac{L_{ext}}{4\pi c R_{ext}^2} \frac{1}{1 + (r/R_{ext})^{n_{ext}}}, \quad (8)$$

where “ext” can be either dusty torus or BLR, and $n_{ext} = 3$ and 4 are used correspondingly for BLR and dusty torus, r - is the distance of the emission region from the central source. The distance of BLR and dusty torus from the central source is calculated as $R_{BLR} = 10^{17} (L_{disk}/10^{45})^{0.5} cm$ [27] and $R_{dust} = 0.4(L_{disk}/10^{45})^{0.5} (1500K/T_{dust})^{2.6} pc$ [28]. The luminosity of external photons is calculated as [29]

$$L_{ext}(\mathcal{E}) = \frac{15}{\pi^4} \xi_{ext} L_{disk} \frac{(\mathcal{E}/kT_{ext})^4}{\exp[\mathcal{E}/kT_{ext}] - 1}, \quad (9)$$

where ξ_{ext} is a fraction of the reprocessed emission from the accretion disk (L_{disk}), which can be defined by the user (the typical values are $\xi_{dust} = 0.3$, $\xi_{BLR} = 0.6$) and T_{ext} is the temperature. All the external photon fields are transferred to the jet frame taking into account the Doppler boosting factor.

Electron spectral models: The exact mechanism responsible for the acceleration of electrons in blazar jets is still under debate. Several different acceleration mechanisms are proposed, which can explain the formed spectra of particles in the jets. The domination of different acceleration and cooling processes can form various spectra for emitting particles. For example, one of the most expected mechanisms for electrons acceleration is the diffuse shock acceleration (Fermi acceleration) which predicts a power-law spectrum [30], or when the efficiency of shock acceleration mechanism is considered, this spectrum becomes a power-law with an exponential cutoff distribution [31]. When the accelerated particles cool in reasonable timescales, then a broken power-law electron spectrum can be formed [31][32]; and when the main particle acceleration mechanism is stochastic acceleration, then a log-parabolic spectrum will be formed [33]. In order to keep the generality, the spectra for emitting particles can be defined as

- power-law

$$N(E_e) = W_e \left(\frac{E_e}{E_0} \right)^{-\alpha}, \quad (10)$$

where W_e is the total energy in electrons, E_e and E_0 are the electron energy and the normalization, and α is the slope,

- broken power-law

$$N(E_e) = \begin{cases} W_e \left(\frac{E_e}{E_0} \right)^{-\alpha_1} & E_e \leq E_{br}, \\ W_e \left(\frac{E_{br}}{E_0} \right)^{\alpha_2 - \alpha_1} \left(\frac{E_e}{E_0} \right)^{-\alpha_2} & E_e > E_{br} \end{cases}, \quad (11)$$

where E_{br} is the break energy, α_1 and α_2 are the power-law indices before and after the break, respectively,

- exponential cutoff power-law

$$N(E_e) = W_e \left(\frac{E_e}{E_0} \right)^{-\alpha} \exp \left(- \left(\frac{E_e}{E_{cutoff}} \right)^\beta \right), \quad (12)$$

where E_{cutoff} is the cutoff energy and β is the rate of exponential decay, and

- log-parabola

$$N(E_e) = W_e \left(\frac{E_e}{E_0} \right)^{-\alpha - \beta \log \left(\frac{E_e}{E_0} \right)}, \quad (13)$$

where β defines the curvature in the spectra.

Optimization: After defining the radiative models and distribution of underlying particles, the last phase is to optimize the free parameters. Before starting the fit, the initial values for all considered parameters should be provided together with the parameters known from the observations (e.g., size of the emission region, Doppler factor etc.). Also, the parameters for the external photon field(s) should be provided and defined which fields should be considered for the IC calculations. In order to optimize the step for providing initial parameters for the electron energy distribution (EED) and magnetic field, after launching the program an interactive window will open, which allows to change the parameters manually in order to reach reasonable fit to data (visual). This optimization can be also done with the defined Nelder-Mead algorithm. The fitting can be performed in fast ($nwalkers = 32$, $nburn = 10$, $nrun = 10$, $thread = 4$) and slow ($nwalkers = 64$, $nburn = 100$, $nrun = 100$, $thread = 4$) modes, which use different division of the provided range of parameters. The *nwalkers* parameter is defined in Goodman & Weare [21], which specifies how many walkers will be used in the sampling procedure; *nburn* specifies how many steps should be run as burn-in and after *nburn* steps the sampler is reset and the chain history discarded; the *nrun* specifies how many steps to run after the burn-in and save these samples in the sampler object, and the *thread* is the number of threads to use for sampling [5]. The user can choose which mode is better, depending on the number of data points and free parameters. Sometimes the emission from distant blazars can be absorbed, when the produced photons interact with extragalactic background light (EBL) photons and in the modeling this absorption should be taken into account. The code includes several models for EBL absorption (e.g., Franceschini (2008) [34], Dominguez (2011) [35], etc.) which can be defined by the user.

4. Application to model the SEDs of Mkn 501 and PKS 0537-441

In order to demonstrate how the code works, the SEDs of Mkn 501 and PKS 0537-441 blazars are modeled. These two sources are selected from both types of blazars, the first one is a BL-Lac, and the second one is a FSRQ to demonstrate the data fitting using both SSC and EIC models.

Mkn 501 at a redshift $z = 0.034$ is among the most studied BL-Lacs in the γ -ray band [36]. It shows variable emission in almost all bands: sometimes simultaneous, but in general, time lags between emissions in different bands were observed. For the current study, the simultaneous data observed between 2009 March 15 (MJD 54905) to 2009 August 1 (MJD 55044) are used. The emission is assumed to be produced from a region (“blob”) with a size of $R = 1.3 \times 10^{17} \text{ cm}$ and a Doppler factor of $\delta = 12$ [36].

PKS 0537-441 is a bright FSRQ blazar at the distance of $z = 0.896$ [37]. For modeling the averaged spectrum observed during 2008 August 4–2010 February 4 (MJD 546 82–552 31) is used. The blob with a size of $R = 1.6 \times 10^{17} \text{ cm}$ [37] is assumed to move with a bulk Lorentz factor of $\Gamma_{bulk} = \delta = 50$. It is assumed, that the emitting region is outside the BLR and the torus photons are dominating. The torus is assumed to have a blackbody spectrum with a luminosity of $L_{dust} = 3.3 \times 10^{42} \text{ erg s}^{-1}$ and a temperature of $T_{dust} = 3 \times 10^2 \text{ K}$ [37] and fills a volume that for simplicity is approximated as a spherical shell with a radius of $R_{dust} = 0.4(L_{disk}/10^{45})^{0.5}(1500\text{K}/T_{dust})^{2.6} \text{ pc}$ [28].

The broadband SEDs of Mkn 501 and PKS 0537-441 are shown in fig. (1), where the data are from [36] and [37], respectively. The data are modeled in the framework of one-zone leptonic model involving synchrotron, SSC and EIC processes. Usually the spectra of BL-Lacs are better described when IC scattering of synchrotron photons are considered (SSC) instead of the large Compton dominant observed for FSRQs (> 100 in these cases), when external photons are considered (EIC) [17]. Therefore, for modeling of the SEDs of Mkn 501 and PKS 0537-441, the synchrotron/SSC and synchrotron/EIC scenarios have been correspondingly considered.

The electron energy density responsible for the nonthermal emission is assumed to be broken power-law, which is naturally formed from the cooling of relativistic electrons [31][32]. The prior likelihood, our prior knowledge of the probability distribution of a given model parameter, and the data likelihood functions are passed on to the emcee sampler [38] function for an affine-invariant MCMC run. There are seven model free parameters (e.g. the magnetic field, electron spectral indices etc.) and for each of them physically reasonable ranges are provided: $1 \leq (\alpha_{1,2}) \leq 10$, $0.511 \text{ MeV} \leq E_{(br, \min, \max)} \leq 1 \text{ TeV}$, and W_e and B are defined as positive parameters. Using MCMC fitting, the predicted emission spectra for each combination of the seven parameters are calculated and combined with the data, and then the maximum log-likelihoods are obtained. Besides the best guess values of the parameters that the code provides in the end, also the uncertainties of those parameters are estimated.

5. Result and Discussion

The results of SEDs modeling are shown in fig. (1) and the estimated parameters are in table (1). In addition, the posterior distributions of spectral model parameters are obtained, and two of them with several statistics of the posterior distribution and parameter values with respect to the step number of the chains are depicted in fig. (2). Since a strong EBL absorption is expected for the distance of PKS 0537-441 ($z = 0.896$), in the SED modeling the EBL absorption was taken into account using the model of Franceschini (2008) [34].

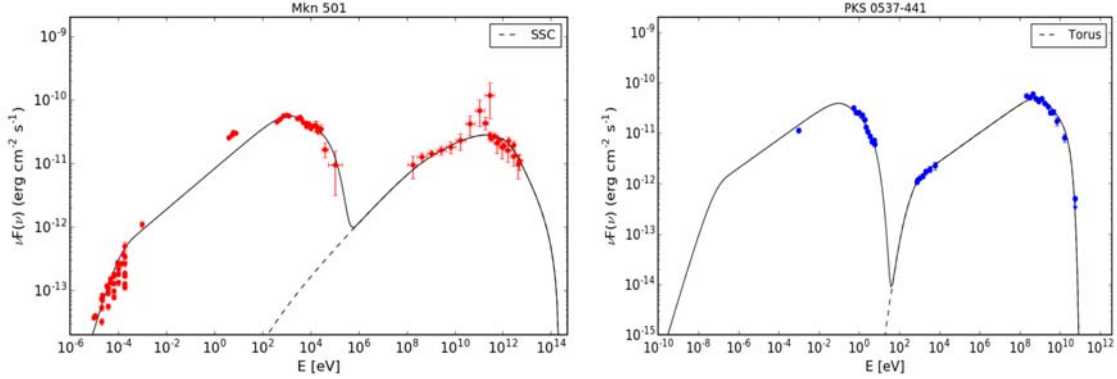


Figure 1: Modeling of the broadband SEDs of Mkn 501 and PKS 0537. Dotted lines show the high-energy models. The model parameters are presented in table (1).

Table 1. Model parameters.

	Parameter	Mkn 501	PKS 0537-441
Doppler factor	δ	12	50
Total electron energy	$W_e \times 10^{50} \text{ erg}$	0.11	2.72
Low-energy electron spectral index	α_1	$2.36^{+0.08}_{-0.05}$	$2.429^{+0.005}_{-0.010}$
High-energy electron spectral index	α_2	3.39 ± 0.01	3.68 ± 0.03
Minimum electron energy	$E_{min}(\text{MeV})$	$126.41^{+19.60}_{-11.20}$	$0.73^{+0.01}_{-0.09}$
Break electron energy	$E_{br}(\text{GeV})$	$431.91^{+30.29}_{-59.43}$	$1.00^{+0.04}_{-0.02}$
Maximum electron energy	$E_{max}(\text{TeV})$	$3.80^{+0.39}_{-0.73}$	$6.05^{+0.03}_{-0.05}$
Magnetic field	$B[\text{mG}]$	$7.95^{+3.77}_{-1.49}$	$67.47^{+0.66}_{-0.52}$
Jet power in magnetic field	$L_B \times 10^{42} \text{ erg s}^{-1}$	0.58	1092.62
Jet power in electrons	$L_e \times 10^{45} \text{ erg s}^{-1}$	0.28	95.69

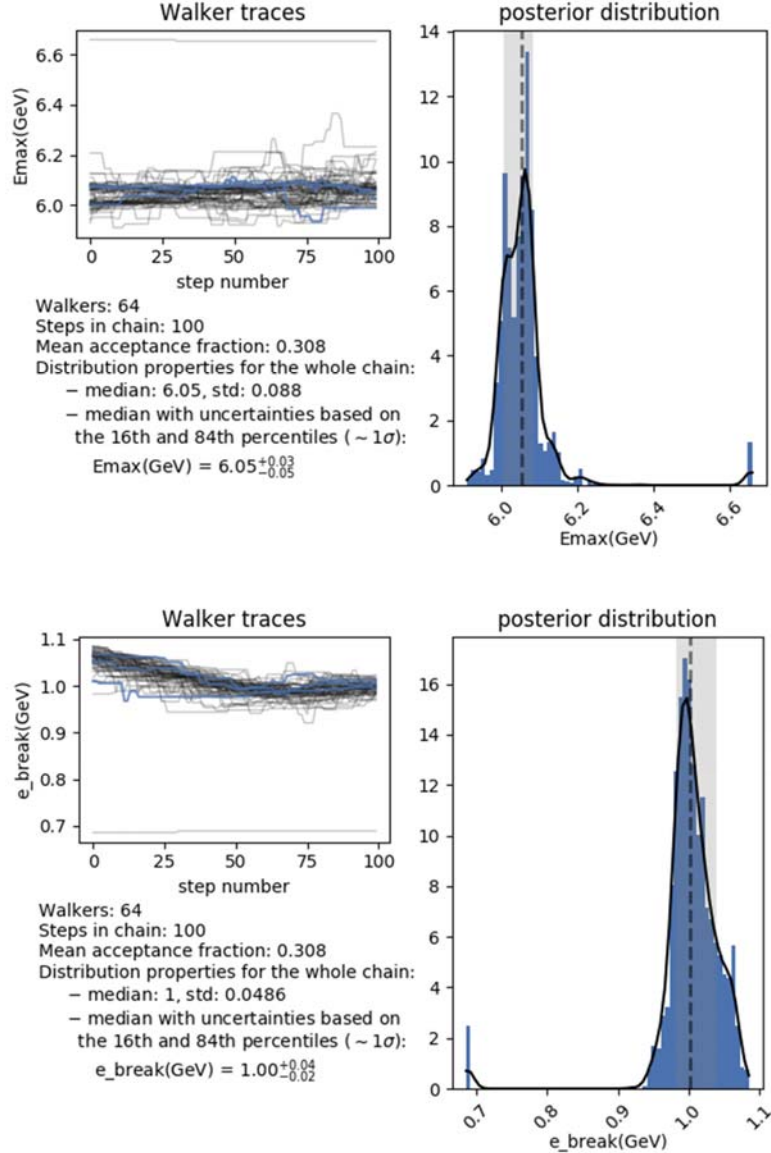


Figure 2. The posterior distributions for E_{\max} and E_{br} parameters of PKS 0537-441 fitting, assessed through MCMC sampling, with several statistical and computational parameters are plotted.

In the modeling of Mkn 501 SED, the observed HE and VHE γ -ray data allowed to constrain the power-law indices of underlying electrons before and after the break: the SED is best modeled when $\alpha_1 = 2.36 \pm 0.07$ and $\alpha_2 = 3.39 \pm 0.01$. As $\alpha_2 - \alpha_1 \approx 1$, this implies, that the break in the spectra of electrons is formed when the cooling of electrons was dominating [39]. The break energy can be constrained by the peaks of the low- and high- energy components and corresponds to $E_{br} \approx 432 \pm 47.2 \text{ GeV}$, showing the particles are effectively accelerated in the jet of Mkn 501. The observed radio flux allows to limit the minimum electron energy by $E_{\min} = 126.4 \pm 16.0$, however the lack of available data in $keV - MeV$ band and large scattering

of radio data points does not allow precise estimation of E_{\min} . This introduces uncertainties in the estimation of the total content of electrons, but even in this case large particle-energy-dominance is found, $U_e/U_B \approx 483$.

In the modeling of the SED of PKS 0537 both SSC and IC scattering of torus photons are considered. In order to explain the data with synchrotron/SSC model, a strong particle dominated jet should be considered, $U_e/U_B \geq 10^4$. At the same time, when the IC scattering of external photons is considered, the data can be explained when the system is nearly in the equipartition, $U_e/U_B \approx 88$. In this case, the X-ray data are used to estimate both $\alpha_1 = 2.43 \pm 0.008$ and $E_{\min} = 0.73 \pm 0.062$. The peak of the low-energy component cannot be well constrained, it varies within $(0.01-1)eV$, and the break energy $E_{br} \approx 1.00 \pm 0.03 GeV$ is constrained by the observed GeV data. The available optical/UV and GeV data points also allow to constrain the maximum energy of accelerated electrons, $E_{\max} = 6.05 \pm 0.04 GeV$.

The large uncertainties in the estimations of some parameters (e.g. $E_{\min,br}$ for Mkn 501 or $E_{\min,br}$ and α_2 for PKS 0537) are related with the lack of data or large scattering in the measurements. For example, in the case of PKS 0537, the radio data are missing, so with X-ray data the combination of α_1 and E_{\min} parameters can be estimated, which results in uncertainties for both parameters. On the other hand, the archival data available from multiple radio observations of Mkn 501 makes it significantly harder to estimate E_{\min} accurately. However, these difficulties are present in not only the proposed method, but also are common in all numerical techniques applied to model the observed spectra of blazars. In the best cases, when a large amount of simultaneously observed data is available, all the model free parameters can be estimated with a high accuracy.

The parameters presented in table (1) allow to not only constrain the energy distribution of emitting particles and consequently understand the acceleration and radiation processes of the particles, but also to estimate several important parameters that characterize the jet. For example, the jet power in the form of magnetic field and electron kinetic energy can be calculated by $L_B = \pi c R_b^2 \Gamma^2 U_B$ and $L_e = \pi c R_b^2 \Gamma^2 U_e$ [40], respectively, which are given in table (1). It is interesting to compare the obtained values of L_e and L_B (table (1)) with those estimated in [36] and [37], where the model free parameters were estimated by different methods. For Mkn 501, the corresponding parameters are $L_e = 1.1 \times 10^{44} erg s^{-1}$ and $L_B = 2 \times 10^{42} erg s^{-1}$ and for PKS 0537 are $L_e = 1.2 \times 10^{46} erg s^{-1}$ and $L_B = 1.9 \times 10^{46} erg s^{-1}$. This shows that the results obtained here are in agreement with the previously obtained ones, which once more illustrates the accuracy of the proposed method. These estimations also allow to estimate the total jet luminosity ($L_{jet} = L_e + L_p + L_B$), assuming one proton per relativistic electron [40][41], $L_{jet} = 1.0 \times 10^{45} erg s^{-1}$ and $L_{jet} = 3.82 \times 10^{49} erg s^{-1}$ for Mkn 501 and PKS 0537, respectively. This shows that the fundamental properties of the sources too can be estimated based on the obtained results, which are crucial for understanding different components of the sources.

6. Conclusion

One of the most effective ways of investigating the nonthermal processes in various astrophysical sources is through modeling of the observed multiwavelength data. The accurate interpretation of the observed data, i.e., finding of the parameters that explain the observed data statistically better is one of the actual problems in modern multiwavelength astrophysics. In this paper, a new code that uses MCMC method to constrain the model free parameters is presented. It is based on the affine-invariant ensemble sampling algorithm and is a powerful method, when the model consists of a large number of free parameters. As a practical application of the algorithm, the multiwavelength data from the observations of very powerful blazars Mrk 501 and PKS 0537 are discussed; it shows how the parameters characterizing the emitting particles as well as the jet can be estimated. The primary application of the code is to model the multiwavelength emission from blazars, but since various radiative models of electrons are included, it can be successfully used in the modeling of the spectra of other astrophysical sources as well.

References

- [1] Ch., Beckmann V. and Shrader.,(Active Galactic Nuclei, 2012).
- [2] C. M. Urry, P. Padovani. 107, 803, PASP, 1995.
- [3] A. Tramacere, P. Giommi, M. Perri, F. Verrecchia, & G. Tosti, 501, 879, A&A, 2009.
- [4] A. Tramacere, E. Massaro, & A. M. Taylor, 739, 66, ApJ, 2011.
- [5] V. Zabalza, 34, 922Z, ICRC, 2015.
- [6] A. A. Abdo, M. Ackermann, M. Ajello, et.al. 716,30, ApJ, 2010.
- [7] G. Ghisellini, L. Maraschi, A. Treves, 146, 204, A&A, 1985.
- [8] L. Maraschi, G. Ghisellini, A. Celotti 397, L5, ApJ, 1992.
- [9] M. Sikora, M. C. Begelman, M. J. Rees 421, 153, ApJ, 1994.
- [10] G. Ghisellini, F. Tavecchio 397, 985, MNRAS, 2009.
- [11] M. Petropoulou, S. Dimitrakoudis, P. Padovani, A. Mastichiadis, E. Resconi. 448, 2412-2429, MNRAS, 2015.
- [12] K. Mannheim , & P. L. Biermann, 253, L21, A&A, 1992.
- [13] F. A. Aharonian, 5, 377, NewA, 2000.
- [14] A. M u cke, & R. J. Protheroe, 15, 121, Astroparticle Physics, 2001.
- [15]M. B o ttcher, A. Reimer, K. Sweeney, A. Prakash. 768, 54, ApJ, 2013.
- [16] M. Petropoulou, & C. D. Dermer, 825, L11, ApJL, 2016.
- [17] M. Sikora, Ł. Stawarz, R. Moderski, K. Nalewajko, G. M. Madejski 704, 38, ApJ, 2009.
- [18] M.H. Ulrich, L. Maraschi, C.M. Urry. 35, 445-502, ARA&A, 1997.
- [19] J.G. Kirk, F.M. Rieger, and A. Mastichiadis, 333, 452–458, A&A, 1998.
- [20] D. Wraith, M. Kilbinger, K. Benabed, O. Capp e , J.-F. Cardoso, G. Fort, S. Prunet, and C. P. Robert. 80(2):023507, Physical Review D, 2009.
- [21] J. Goodman, & J. Weare, 5, 65, Comm. App. Math. Comp. Sci., 2010.
- [22] D. Foreman-Mackey, D.W. Hogg, D. Lang, & J. Goodman 125, 306, PASP, 2013.
- [23] D. MacKay, Information Theory, Inference, and Learning Algorithms., (Cambridge University Press, 2003).
- [24] F. A. Aharonian, S. R. Kelner, A. Y. Prosekin 82, 043002, Phys. Rev. D, 2010.
- [25] J. D. Finke, C. D. Dermer, M. B o ttcher 686, 181, ApJ, 2008.
- [26] M. Hayashida, G. M. Madejski, K. Nalewajko 754, 114, ApJ, 2012.
- [27] G. Ghisellini, F. Tavecchio, L. Maraschi, A. Celotti, T. Sbarrato,. 515, 376, Nature, 2014.
- [28] M. Nenkova, M. M. Sirocky, R. Nikutta, Z . Ivezi c , M. Elitzur, 685, 160, ApJ, 2008.
- [29] C. D. Dermer, M. Cerruti, B. Lott, C. Boisson, A. Zech 782, 82, ApJ, 2014.
- [30] E., Fermi. 75, 1169, Phys. Rev., 1949.
- [31] S. Inoue, F. Takahara 463, 555, ApJ, 1996.
- [32] N. S.Kardashev, 6, 317, Soviet Ast., 1962.
- [33] B. Park, V. Petrosian 446, 699, ApJ, 1995.

- [34] A. Franceschini, G. Rodighiero, M. Vaccari 487, 837, A&A, 2008.
- [35] A. Dominguez, et al. 410, 2556, MNRAS, 2011.
- [36] A. A. Abdo, M. Ackermann, M. Ajello, et al. 727, 129, ApJ, 2011.
- [37] F. D'Ammando, E. Antolini, G. Tosti, et al. 431, 2481, MNRAS, 2013.
- [38] D. Foreman-Mackey, D. W. Hogg, D. Lang, J. Goodman 125, 306, PASP, 2013.
- [39] Takami, Hajime. 355 012025, J. Phys.: Conf. Ser., 2012.
- [40] A. Celotti, G. Ghisellini 385, 283, MNRAS, 2008.
- [41] G., Ghisellini. Radiative Processes in High Energy Astrophysics. Berlin (Springer-Verlag Vol. 873, 2013).
- [42] M. L. Ahnen, S. Anoldi, L. A. Antonelli, 603, A31, A&A, 2017.
- [43] J. Albert, E. Aliu, H. Anderhub, 669, 862., APJ, 2007.
- [44] M. Cerruti, A. Zech, C. Boisson & S. Inoue, 448, 910, MNRAS, 2015.
- [45] G. Ghisellini, L. Maraschi, F. Tavecchio 396, L105., MNRAS, 2009.
- [46] F. Tavecchio, L. Maraschi & G. Ghisellini, 509, 608., APJ, 1998.
- [47] A. Zech, M. Cerruti & D. Mazin, 602, A25, A&A, 2017.